Journal of *Marine Science and Engineering*

MDPI

Article

Investigation into the Synergistic Effects of Sediment Concentration and Particle Size on the Friction and Wear Properties of Nitrile Butadiene Rubber

Lun Wang [1,2,3,*], Xincong Zhou [1,2,3,*], Qipeng Huang [1,2,3], Xueshen Liu [4], Zhenjiang Zhou [1,2,3] and Shaopeng Xing [1,5]

[1] State Key Laboratory of Maritime Technology and Safety, Wuhan University of Technology, Wuhan 430063, China
[2] School of Transportation and Logistics Engineering, Wuhan University of Technology, Wuhan 430063, China
[3] Reliability Engineering Institute, National Engineering Research Center for Water Transport Safety, Wuhan University of Technology, Wuhan 430063, China
[4] School of Mechanical Engineering, Zhengzhou University of Aeronautics, Zhengzhou 450046, China
[5] School of Naval Architecture, Ocean and Energy Power Engineering, Wuhan University of Technology, Wuhan 430063, China
* Correspondence: hqwanglun3792@foxmail.com (L.W.); xczhou@whut.edu.cn (X.Z.)

Abstract: Nitrile Butadiene Rubber (NBR) is commonly used in ships' water-lubricated tail bearings. However, sediment in the water significantly affects these bearings' friction and wear performance. This study investigates NBR test blocks' friction and wear behavior in conjunction with ZCuSn10Zn2 copper ring friction pairs within a sediment-laden water lubrication environment. Two primary factors were considered: sediment particle concentration and sediment particle size. Friction and wear tests were conducted under pure water and sediment-laden conditions using the ZY-1 ring block friction and wear tester. The friction coefficients, wear quantities, and variations in mass concentrations and sediment particle sizes were measured and compared. The surface morphology of the test blocks was analyzed using a laser confocal microscope. The findings indicate that as sediment concentration increases, the particle size's impact on NBR's abrasive wear diminishes. The variation in particle size directly influences the number of particles that penetrate the interface between the friction partners and the nature of three-body wear. Conversely, changes in particle concentration primarily affect the extent of wear; specifically, both the wear volume and the average coefficient of friction of the NBR specimens increase with rising sediment concentration. The wear mechanisms observed on the surface of the NBR test blocks are predominantly characterized by micro-cutting, rolling wear, and the coexistence of both wear modes. This study offers valuable insights for the design and optimization of water-lubricated bearings.

Keywords: nitrile butadiene rubber; sediment content; particle size effects; friction and wear properties; synergistic effect; wear mechanisms

check for updates

Academic Editor: Vincenzo Crupi

Received: 20 November 2024
Revised: 23 December 2024
Accepted: 27 December 2024
Published: 29 December 2024

Citation: Wang, L.; Zhou, X.; Huang, Q.; Liu, X.; Zhou, Z.; Xing, S. Investigation into the Synergistic Effects of Sediment Concentration and Particle Size on the Friction and Wear Properties of Nitrile Butadiene Rubber. *J. Mar. Sci. Eng.* **2025**, *13*, 33. https://doi.org/10.3390/jmse13010033

Copyright: © 2024 by the authors. Licensee MDPI, Basel, Switzerland. This article is an open access article distributed under the terms and conditions of the Creative Commons Attribution (CC BY) license (https://creativecommons.org/licenses/by/4.0/).

1. Introduction

The Yangtze River, as an essential golden waterway in China, plays a crucial role in developing the Yangtze River Economic Belt, and its shipping value and potential have been fully utilized [1,2]. With the continuous strengthening of national environmental protection policies, green, low-carbon, efficient, and stable shipping has become the primary trend in developing inland vessels. Against this background, how to reduce the environmental

pollution caused by ships during operation has become an urgent problem that needs to be solved. Adopting water lubrication technology instead of traditional lubricating oil has become one of the most effective ways to reduce pollution. This technology utilizes water as the lubricating medium, which can effectively reduce the use of lubricating oil and thus reduce the risk of lubricating oil leakage [3,4]. At the same time, water-lubricated bearings made of NBR have received widespread attention and importance. This material has been widely used in the mechanical fields of ship propellers, ships, and deep-water pumps, with its good wear resistance, corrosion resistance, and self-lubrication performance providing strong support for the long-term stable operation of this equipment [5–8].

A comprehensive investigation of sediment hydraulic transport data in the middle and lower reaches of the Yangtze River has revealed a substantial presence of fine-grained suspended sand [9]. This phenomenon presents a potential risk to vessels employing water-lubricated rubber bearings as propulsion mechanisms, as it may not only degrade bearing performance but also disrupt the efficient and smooth operation of the vessel, potentially reducing its service life [10]. Consequently, it is imperative to investigate further the frictional wear mechanisms of rubber induced by sediment particles to enhance operational efficiency and prolong the service life of ships navigating through sandy waters [11].

Both domestic and international scholars have conducted numerous studies on the friction and wear properties of rubber/complex metal composites, achieving significant advancements in this field. These investigations primarily aim to enhance the tribological properties of rubber through various methodologies, including surface modification [12–17], material filling [18–22], surface coating technology [23–25], and polymer compounding [26–28]. For instance, Alex et al. [29] explored the friction mechanisms between rubber and ice and sand and ice. They discovered a blizzard layer measuring less than 1 mm, which positively influenced friction reduction. Chang et al. [30] analyzed the impact of tire rubber particles on the tribological properties of brake friction materials, demonstrating that variations in particle size significantly affected contact stiffness, platform formation, and wear performance. Wang et al. [31] designed a novel water-lubricated rubber-bearing structure and conducted an in-depth study of its tribological characteristics. Their findings indicate that the coefficient of friction decreased with increasing rotational speed, while the coefficient of friction for rubber bearings with gears increased sharply with rising temperature. Additionally, the coefficient of friction initially increased with load before subsequently decreasing. Yan et al. [32] developed new ultra-high-molecular-weight polyethylene (UHMWPE)/graphite/nitrile rubber structured water-lubricated bearings demonstrating excellent tribological properties. Lv et al. [33] investigated the solution-induced aging and tribological behavior of nitrile rubber in cyclohexane, revealing that wear loss of the NBR samples was minimal at low loads, with the wear mechanism transitioning from mild abrasive wear to severe abrasive wear at elevated loads. Finally, Zafar et al. [34] examined the abrasive and erosive wear properties of WC-12Co microwave cladding, concluding that spalling and carbide fracture were the primary wear mechanisms during erosive wear, and that the presence of nano carbide clusters with low mean degrees of freedom effectively mitigated cracking.

The investigation of the effect of abrasive particle size on rubber friction and wear performance has garnered significant attention from scholars both domestically and internationally. Various experimental methodologies and material systems have been employed to elucidate the influence of abrasive particle sizes on the tribological properties of rubber. For instance, Lee et al. [35] examined the impacts of Al_2O_3 particles on the wear behavior of Viton rubber, utilizing a pin-plate reciprocating tester. Their findings indicate that the particles' irregular cutting and rolling actions contributed to an increase in the friction component, thereby affecting the coefficient of friction. Conversely, Chang et al. [30] explored the relationship between the friction and wear performance of rubber particles of two

sizes in conjunction with brake materials. Their results demonstrate that the high-pressure contact surface generated by smaller rubber particles exhibited a higher wear rate. In comparison, larger particles were associated with reduced friction, wear rates, and brake materials. The results show that the high-pressure contact surface produced by the small rubber particles had a high wear rate, whereas the large-sized particles reduced the friction, wear rate, and brake noise. Shen et al. [36] chose four different AI_2O_3 particles. They investigated the characteristics of the particles on the rubber/stainless steel friction vice, such as the time-varying curve of the friction coefficient, the friction wear morphology and the damage mechanism, and the results show that there were significant differences in the influences of different-sized particles on the wear behavior of the rubber. Walk et al. [37] found a critical value in the abrasive wear process, and that the wear rate no longer changes with the abrasive particle size after exceeding this critical value. Li et al. [38] investigated the effects of four sizes on the frictional wear of rubber, and revealed the relationship between the friction coefficient, wear, and particle size and load. However, all of the above studies considered the effects of working conditions such as medium, load, and speed on their tribological properties in specific environments, and relatively few studies were conducted on the friction and wear of rubber in muddy and sandy environments. Meanwhile, the effect of abrasive particle concentration on rubber's friction and wear performance has also attracted wide attention. Liao et al. [39] studied the tribological properties of rubber in a muddy sand environment, and found that the wear volume and friction coefficient tended to increase slowly and then rapidly with the increase in sand content. Ren et al. [40] investigated the friction and wear performance of ultrafine WC-Co from the three-body wear point of view. For cemented carbide in different particle concentrations, it was found that the wear mechanism mainly depends on the particle hardness rather than the particle concentration. Park et al. [41] investigated the effects of SiO_2 and AI_2O_3 particle-containing media solutions on the wear behavior of rubber sealing materials, and found that there exists a critical concentration, and that the wear volume of the rubber after exceeding this critical concentration increases with the increase in particle size. Liang et al. [42] and others investigated the tribological properties of polyurethane and nitrile rubber in SiO_2-containing environments, revealing the influence of SiO_2 concentration on the wear behavior of rubber.

In systems involving rubber–hard material friction pairs, the issues of damage and wear attributed to various lubricating media have attracted considerable scholarly attention, leading to ongoing advancements in related research. Nonetheless, the influences of sand particle concentration and size on the performances of these friction pairs remain a contentious topic, primarily due to the constraints imposed by experimental conditions and environmental factors, resulting in a lack of consensus in the field. Furthermore, the wear mechanisms associated with rubber/hard material friction pairs are intricately related to the particles' size, concentration, and viscosity; however, existing studies have not sufficiently investigated the dynamic alterations of sand particles as they penetrate the friction interface. Specifically, the processes by which sand particles infiltrate the friction interface, how particle size and concentration variations contribute to wear at the friction interface, and the potential for these factors to precipitate system failure still need to be more adequately understood. Current research predominantly emphasizes the analysis of individual factors, thereby neglecting a comprehensive exploration of the synergistic effects of particle size and concentration on the lubrication wear mechanisms of rubber. Consequently, a thorough investigation into the combined effects of sand particle size and concentration on the lubrication wear performance of rubber, as well as their intrinsic relationships, holds significant theoretical and practical importance. This study systematically evaluates the impacts of varying sand concentrations and particle

sizes on the tribological behavior of NBR utilizing ring-block friction and a wear tester. The focus is placed on the alterations in the friction coefficient, wear volume, surface morphology, and wear mechanisms of NBR induced by these two factors. The findings of this research offer critical theoretical insights relevant to enhancing the bearing wear resistance, improving pollution-resistant design capabilities, accurately regulating wear mechanisms, and bolstering environmental adaptability.

2. Materials and Methods

2.1. Test Materials

This study investigates the NBR test block and the copper ring (ZCuSn10Zn2) as the primary subjects of analysis. The aim is to replicate the conditions experienced by water-lubricated rubber bearings in an environment containing sand particles, as depicted in Figure 1a,b. The dimensions of the NBR test block are as follows: a length of 15.5 mm, a width of 6.5 mm, and a height of 10 mm, with the block provided by Hebei Hetzel Rubber and Plastic Products Co. (Hengshui City, Hebei Province, China). The copper ring has an outer diameter of 35 mm and a thickness of 10 mm, produced by Shanghai Kai Rin Metal Materials Co. (Jinshan District, Shanghai, China). To mitigate the influence of surface roughness on the experimental results, the surfaces of each test group were polished prior to testing. The surface roughness of the NBR specimen and the copper ring was assessed using a laser interference displacement sensor (L1-3, Huazhong University of Science and Technology, China). The surface roughness (Sa) of the NBR specimen was determined to be 1.11 ± 0.2 μm, while the surface roughness (Sa) of the copper ring (ZCuSn10Zn2) was measured at 0.55 μm. The principal mechanical properties of the NBR specimen blocks and copper rings are summarized in Table 1.

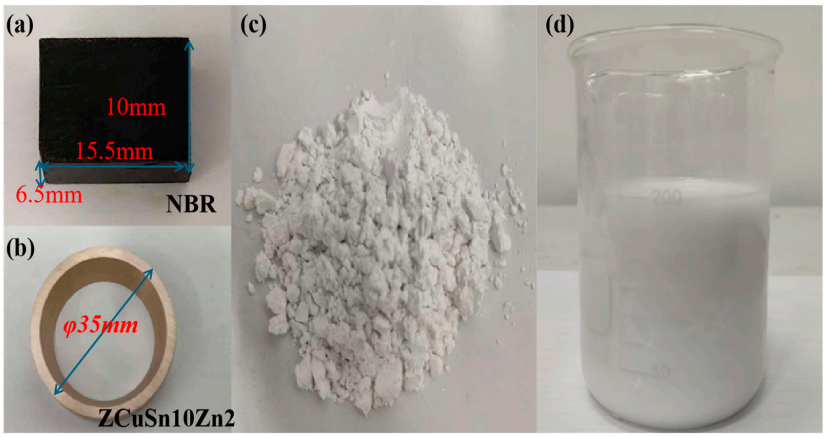


Figure 1. Schematic diagram of test materials. (**a**) NBR test block sample, (**b**) copper ring sample, (**c**) SiO_2 powder sample, (**d**) solution.

Table 1. Main physical properties of NBR and copper ring ZCuSn10Zn2.

Materials	Yield Strength (MPa)	Tensile Strength (MPa)	Young's Modulus E (Gpa)	Density ρ (g/cm^3)	Hardness	Elongation Δ (%)
NBR	-	≤30	5.83	1.38	75 (ShoreA)	≥450
ZcuSn10Zn2	168	≥245	113.4	8.8	154 HV	≥6

This study utilized standard-sized sediment supplied by Henan Changtai Water Purification Materials Co., Ltd., located in Zhengzhou City, Henan Province, China.This sediment comprises hard, abrasion-resistant, and chemically stable silicate minerals, predominantly SiO_2, characterized by a milky white coloration, as depicted in Figure 1c,d. The experiment employed SiO_2 particles with varying particle sizes of 160, 200, 325, 400,

600, 1000, and 3000 mesh, corresponding to average particle sizes of 96, 75, 45, 38, 25, 15, and 5 μm, respectively. The standard deviation between the original and average particle sizes was less than 5%. Aqueous sediment solutions with varying concentrations were prepared to replicate actual environmental conditions, with mass fraction concentrations of 1.5%, 3%, 4.5%, 6%, 7.5%, and 9%. Figure 2 illustrates the microscopic morphology of four representative SiO_2 particles.

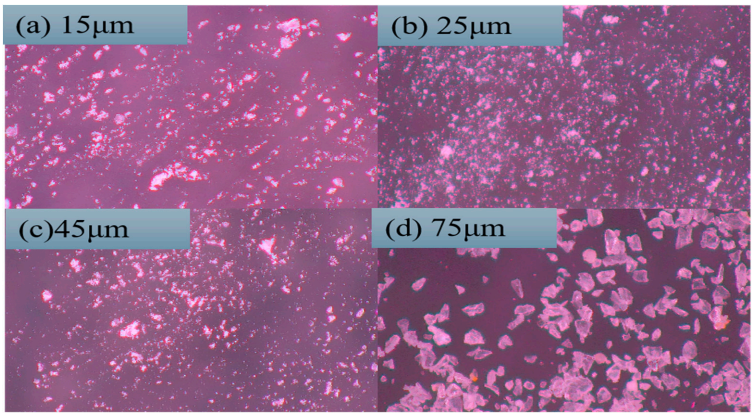


Figure 2. Typical micrographs of four sediment particles of different sizes.

2.2. Test Method and Procedure

The experiment was conducted utilizing ring-block friction and a wear tester (ZY-1 type, China), independently developed by Wuhan University of Technology, as depicted in Figure 3. The test aimed to simulate the sliding behavior of water-lubricated rubber bearings in a muddy environment through the ring-block apparatus. In this setup, the upper specimen, composed of NBR, remained stationary within the medium. In contrast, the lower specimen, a copper ring, was affixed to a rotating shaft powered by a dedicated motor. A lubrication tank is integrated into the test bench, facilitating water lubrication under varying sediment particle sizes and concentrations under sandy water conditions. The water tank is sealed at both the front and rear to ensure continuous contact with the shaft, and it is equipped with fastening screws at the bottom to prevent any relative movement during spindle rotation. The loading force is continuously monitored throughout the test using radial sensors, while the friction force is assessed via transverse sensors. The data collected during the experiment are displayed, stored, and recorded in real-time through the Donghua Dynamic Signal Test and Analysis System (DH5922N, Jiangsu Donghua Testing Technology Co., Ltd., Jiangsu Jinjiang City, China). During the experimental procedure, a small agitator is employed to generate a robust flow through mechanical rotation, thereby inducing vigorous agitation of the sediment particles within the water and enhancing the turbulence of the water flow. This mechanism effectively prevents the sediment particles from settling. The agitator continuously acts on the aqueous sediment solution to ensure the particles remain uniformly suspended throughout the test. Furthermore, the ring-block friction pair utilized in the experiment is fully immersed in the water tank, providing direct contact between the friction pair and the sediment particles in the aqueous solution. The sediment particles interact with the friction surfaces throughout the friction process, simulating the friction mechanisms and wear under real-world conditions.

In this study, we conducted two comparative experiments to investigate the synergistic mechanisms underlying the tribological wear characteristics of NBR under water lubrication conditions, considering various influencing factors, including sand particle concentration, size, sliding speed, and load.

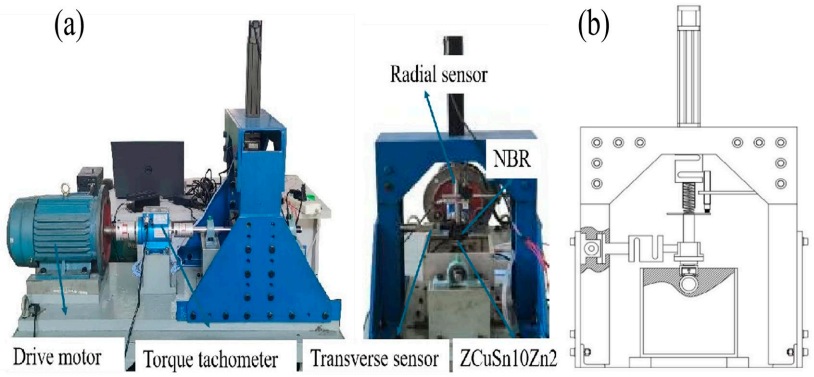


Figure 3. Schematic diagram of friction wear tester. (**a**) Schematic diagram of the testing machine, (**b**) principle diagram of the loading mechanism.

The initial series of experiments was designed to examine the influence of sliding speed and load on NBR's friction and wear characteristics in a muddy environment. A total of twelve distinct rotational speeds were employed during the tests, precisely 30, 60, 120, 180, 240, 300, 360, 420, 600, 800, 1000, and 1200 r/min, which corresponded to linear velocities of 0.055, 0.11, 0.22, 0.33, 0.44, 0.55, 0.66, 0.77, 1.1, 1.47, 1.83, and 2.2 m/s, respectively. Concurrently, the applied loads were established at four levels of 10, 25, 40, and 55 N, resulting in specific pressures of 0.15, 0.38, 0.61, and 0.84 Mpa. Each friction test included a 30 min break-in period, during which the operation at each linear velocity lasted 6 min, and each phase was replicated three times. The sediment water utilized in the experiments had a mass concentration of 6%. The sediment particle sizes were categorized as 5, 15, 25, 38, 45, 75, and 96 μm, corresponding to sediment particle size classifications designated as Type-1, Type-2, Type-3, Type-4, Type-5, Type-6, and Type-7.

Group 2 aimed to examine the influences of sediment concentration and particle sizes on NBR's friction and wear characteristics. The tests were performed under a load of 25 N and a linear velocity of 0.55 m/s to replicate various sedimentary environments. The study encompassed six sediment concentrations (1.5%, 3%, 4.5%, 6%, 7.5%, and 9%) and seven sediment particle sizes (5, 15, 25, 38, 45, 75, and 96 μm), thereby incorporating a range of particle sizes.

The width and depth of the wear track on the sample block were measured using a laser confocal microscope. Based on the principle of integral calculus, the area of the material wear profile was approximated as the sum of an infinite number of very narrow rectangular areas, each with a minimum width of Δl = 3 μm. The laser confocal plane resolution was set to 3 μm, and the formula for the area of the rectangular region Sx with width Δl is [43]

$$S_{\mathrm{x}} = \int_{l_x}^{l+\Delta l_x} f(l_x)dx(x = 1,2,3\ldots,n) \tag{1}$$

The cross-sectional area of the scratch Swear is

$$S_{\mathrm{wear}} = \sum_{1}^{n=\frac{w}{\Delta l}} S_x \tag{2}$$

The wear volume of the specimen is

$$V = L \times S_{\mathrm{wear}} = L \times \sum_{1}^{n=\frac{w}{\Delta l}} \int_{l_x}^{l_x+\Delta x} f(l_{\,x})dx(x = 1,2,3,\ldots,n) \tag{3}$$

In this formula, V (mm^3) represents the wear volume, Swear is the cross-sectional area of the wear track, W (μm) is the width of the wear track, $f(l_x)$ (μm) is the depth value of the wear track at point x along the width, and L (mm) is the length of the wear track.

2.3. Measurement Techniques

During the testing procedure, a transducer integrated into the testing apparatus quantifies the expected load and torque exerted between the friction pair, and we can subsequently calculate the coefficient of friction by use of Equation (4),

$$\mu = \frac{T}{r \cdot N} \tag{4}$$

where μ is the coefficient of friction, T is the torque in N·m, r is the radius of rotation of the friction pair in mm, and N is the leading force in N.

During the experimental procedure, a new NBR test block and a ZcuSn10Zn2 copper ring were utilized for each set of test conditions. To enhance the reliability of the test results, all experiments were conducted in triplicate to mitigate the impacts of random variables. Upon completion of the tests, the surface morphologies of the test samples were assessed using a laser confocal microscope (VK-X1000, KEYENCE, Osaka, Japan), allowing for the acquisition of critical data, including the morphology, wear volume, and surface characteristics of the samples.

3. Result and Discussion

3.1. Effect of Applied Load and Sliding Speed on the Coefficient of Friction

Figure 4 presents the relationship between the friction coefficient and sliding speed across various load conditions. The data illustrated in the figure indicate that the friction coefficient experiences a substantial decrease with an increase in sliding speed, followed by a stabilization phase. This relationship closely aligns with the classical Stribeck curve [44], suggesting that the trend of the friction coefficient about sliding speed remains unaffected by the presence of sediment.

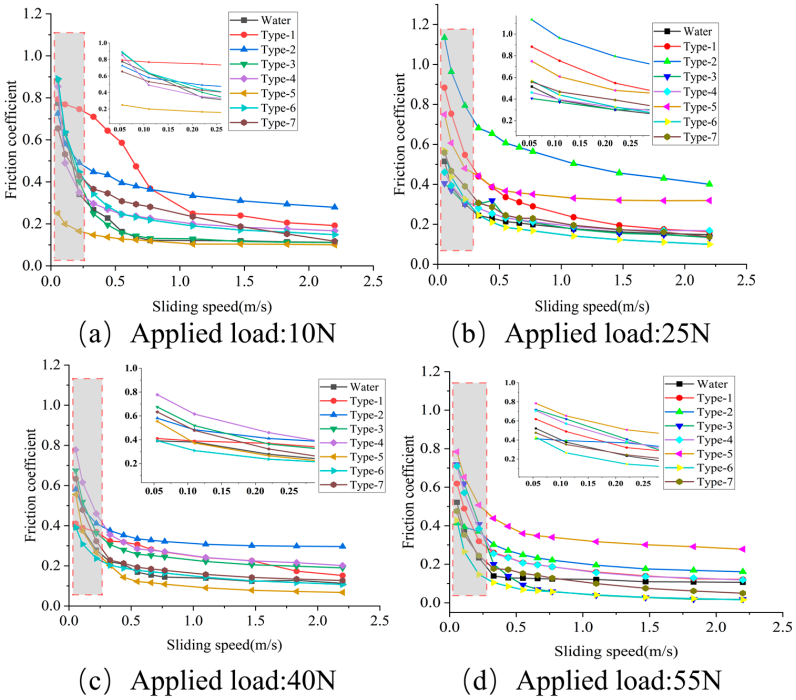


Figure 4. Average friction coefficient variation results of NBR specimens under different loads and sliding velocities.

3.2. Particle Size Effect Analysis

3.2.1. Trend Analysis of Friction Coefficient Under the Influence of Particle Size

As illustrated in Figure 5, the coefficient of friction exhibited a trend of initially increasing and subsequently decreasing with the escalation of particle size at a sediment concentration of 1.5%. Specifically, at this concentration, the average friction coefficient reached its maximum value of approximately 0.422 at a particle size of 75 μm, which is 2.36 times greater than the value observed at a particle size of 5 μm. This phenomenon can be attributed to the behaviors of smaller particles, which tend to roll within the friction apparatus, resulting in minimal surface damage to the NBR material. Consequently, the friction coefficients for particle sizes ranging from 5 to 38 μm are generally lower than those for sizes between 45 and 96 μm. In contrast, larger particles exhibit a higher friction coefficient due to their size being significantly more prominent than the thickness of the water film. This disparity means that only a limited number of sediment particles engage with the friction apparatus, while the larger particles obstruct the relative sliding motion between the friction ring components. This obstruction necessitates a greater shear force for relative motion. Furthermore, in environments with larger particles, the interaction between the particles and the copper ring and the rubber–particle–copper ring interactions are characterized by a pronounced overall increase in the average friction coefficient compared to environments with particle sizes ranging from 5 to 38 μm [45].

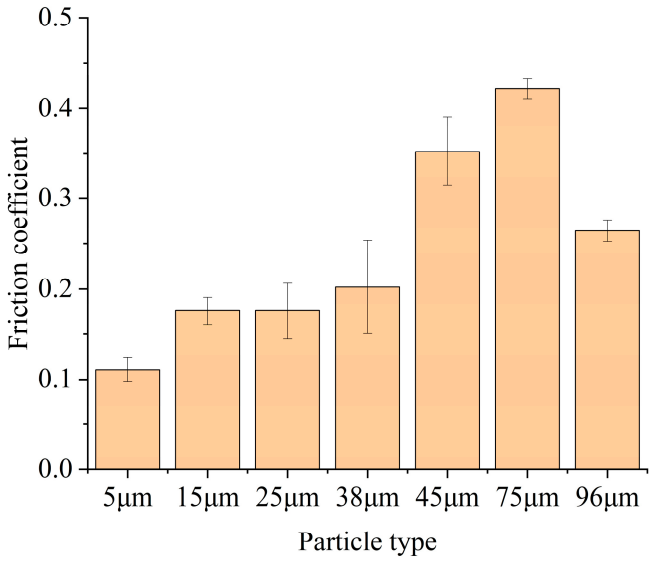


Figure 5. Friction coefficient results under the influence of particle size.

3.2.2. Analysis of the Amount of Wear Under the Influence of Particle Size

Figure 6 illustrates the impacts of varying particle sizes on the wear volume of NBR. The data presented in this figure indicate that the size of sand particles significantly influences rubber wear, mainly when the sand concentration is constant. Specifically, at a sand concentration of 1.5%, NBR wear is lower in the 5 μm environment, higher in the 75 μm environment, and decreases again in the 96 μm environment (refer to Figure 6a). At a sand concentration of 3%, NBR wear is lower in the 15 μm environment and higher in the 75 μm environment (see Figure 6b). Similarly, at a sand concentration of 4.5%, NBR wear is lower in the 5 μm environment and higher in the 75 μm environment (see Figure 6c). This trend persists at a sand concentration of 6%, where wear is lower in the 5 μm environment and higher in the 75 μm environment (see Figure 6d). At a concentration of 7.5%, the wear of NBR continues to be lower in the 5 μm environment and higher in the 75 μm environment (see Figure 6e). Finally, at a sand concentration of 9%, the wear of NBR is again lower in the

5 μm environment and higher in the 75 μm environment (see Figure 6f). The underlying rationale for these observations is that, at a constant concentration, smaller particles tend to create a thicker water film within the lubricating aqueous solution. This water film has a specific load-bearing capacity, reducing the direct contact between the particles and the rubber surface, thereby mitigating wear. Consequently, smaller particles lessen the wear of NBR samples under specific sand concentrations. As the sand concentration increases, the number of sand particles in the lubricating liquid also rises, gradually intensifying the "grinding wheel effect" between the friction pairs. This effect exacerbates the wear processes associated with interactions between rubber and particles and between rubber, particles, and copper rings, resulting in a significant increase in wear. However, when the sand concentration becomes excessively high, and the particle size is large, the increased number of particles and their frequency of interaction with the material surface do not necessarily lead to increased wear. This phenomenon occurs because larger particles encounter challenges entering the contact region of the friction pairs, leading to increased interference among the particles. Consequently, their frequency of entry into the contact region diminishes, which can result in reduced wear under specific size or concentration conditions. Therefore, in engineering practice, it is imperative to prevent the ingress of large, hard sand particles and high concentrations of sand into the contact region of water-lubricated rubber bearings. This precaution is essential for minimizing surface wear at the rubber–metal interface, and effectively extending the service life of the bearings.

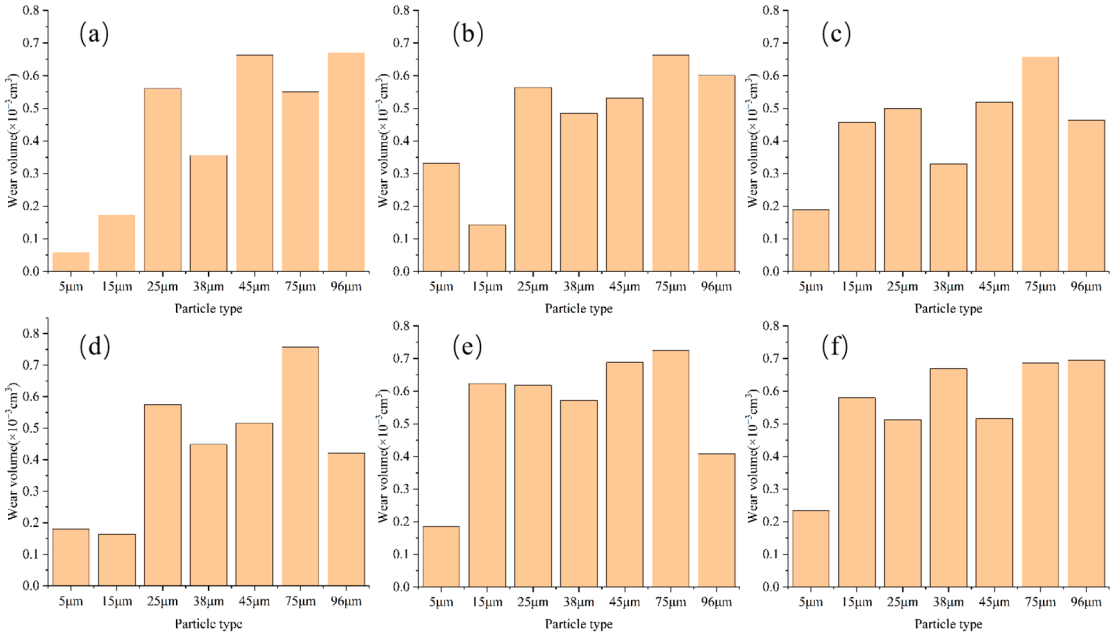


Figure 6. Wear volume under the influence of particle size. (**a**) At 1.5% sediment concentration, (**b**) at 3% sediment concentration, (**c**) at 4.5% sediment concentration, (**d**) at 6% sediment concentration, (**e**) at 7.5% sediment concentration, (**f**) at 9% sediment concentration.

3.2.3. Surface Morphology Analysis Under the Influence of Particle Size

The surface morphology of the NBR sample was analyzed using a laser confocal microscope. Figure 7 illustrates the findings related to the wear surface morphology under specific experimental conditions: a loading force of 25 N, a sliding speed of 0.55 m/s, and a sediment concentration of 6%. The results presented in Figure 7 demonstrate that variations in particle size significantly affect the wear outcomes of the NBR test block. Notably, smaller sediment particles are associated with lighter wear coloration on the surface of the NBR test block. Conversely, an increase in sediment particle size correlates with darker wear

coloration, leading to pronounced grooves and pits on the surface and the entrapment of sediment particles within the rubber matrix.

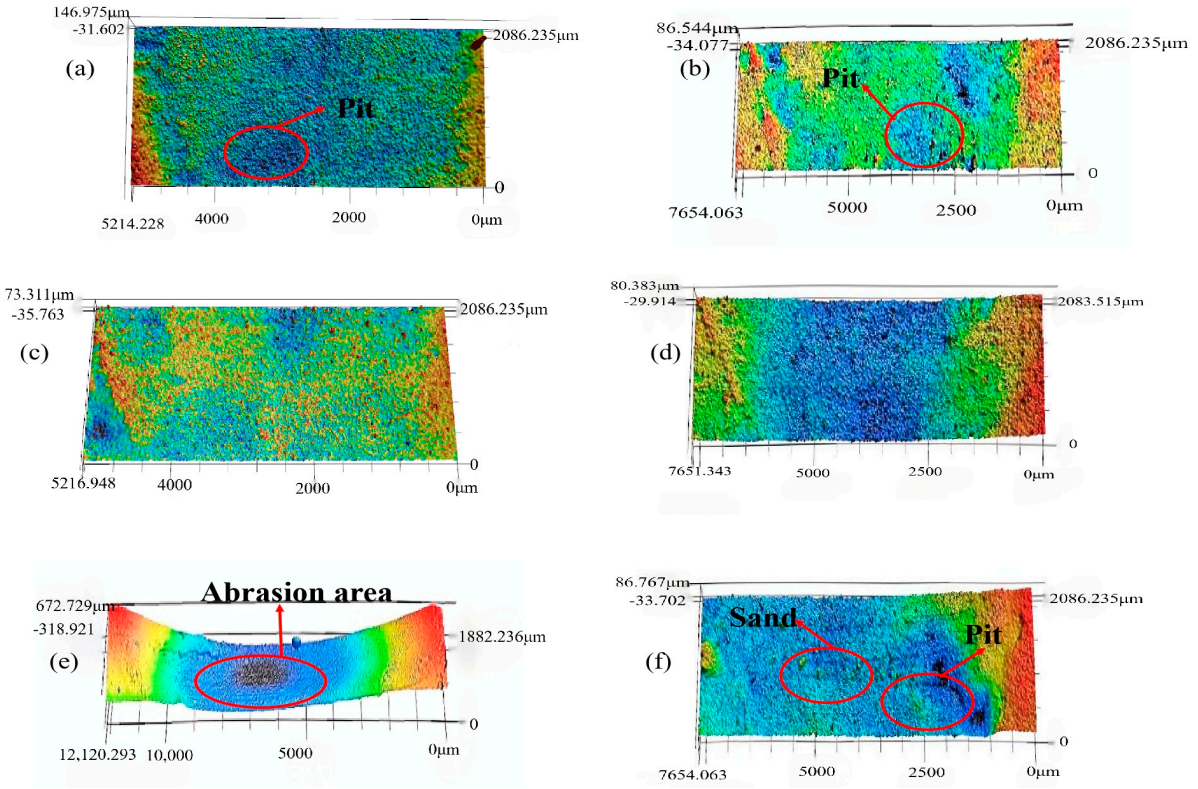


Figure 7. Wear surface morphology under the influence of particle size. (**a**) At particle size 5 μm, (**b**) at particle size 15 μm, (**c**) at particle size 25 μm, (**d**) at particle size 38 μm, (**e**) at particle size 45 μm, (**f**) at particle size 75 μm.

When the mass concentration of the sediment solution is held constant, the wear of NBR is less pronounced with smaller particle sizes. This phenomenon can be attributed to the interaction of water flow, where the size of the abrasive particles is comparable to the thickness of the water film. In such cases, most hard particles traverse the surface of the NBR/copper ring friction sub-surface in a rolling motion, resulting in a diminished micro-cutting effect associated with smaller particle sizes. Conversely, in environments characterized by larger particle sizes, the particles' dimensions significantly exceed the water film's thickness. Consequently, these larger particles cannot penetrate the friction interface, with only a limited number becoming embedded on either side of the NBR friction surface due to the applied loading force. This embedding leads to the formation of micro-convex peaks on the friction surface, facilitating two forms of abrasive cutting effects involving rubber–particle interactions and rubber–particle–copper ring interactions. As a result, the wear effect is more pronounced in environments with larger particle sizes.

3.2.4. Wear Mechanism Analysis Under the Influence of Particle Size

The experimental investigation into the impact of varying sand particle sizes on NBR performance reveals significant differences in the degree of penetration of sand particles within the friction pair. These differences lead to notable variations in the friction coefficient, wear volume, and wear surface morphology. In environments characterized by small particle sizes (5 μm), the dimensions of the sand particles in the slurry solution are comparable to the thickness of the water film, thereby establishing a mutual constraint relationship between the two. Under these conditions, the wear volume is minimal. During the wear process, the slurry flow and shaft transport many small particles along the rubber

surface. Due to the viscoelastic properties of NBR, some particles experience micro-cutting and become embedded in the rubber surface, forming small micro-peaks. These micro-peaks exert a negligible overall destructive effect on the copper ring and the rubber. Instead, they reduce wear between the rubber and the copper ring, providing a certain degree of wear protection. Conversely, when the sand particle size exceeds 5 μm, the particle dimensions significantly surpass the thickness of the water film, disrupting the dynamic equilibrium between the water film thickness and the sand particle size. Under load, a limited number of hard particles are forced into the friction pair, creating large micro-peaks on the rubber surface. At this juncture, the wear mechanism transitions to cutting effects that involve interactions between rubber and particles and between rubber, particles, and the copper ring. Furthermore, some particles are crushed due to the influence of loading forces and other factors, subsequently being carried away by the water flow and the shaft. This continuous dynamic process culminates in forming various types of concave pits and material wear on the surface of the NBR sample, as illustrated in Figure 8b [46].

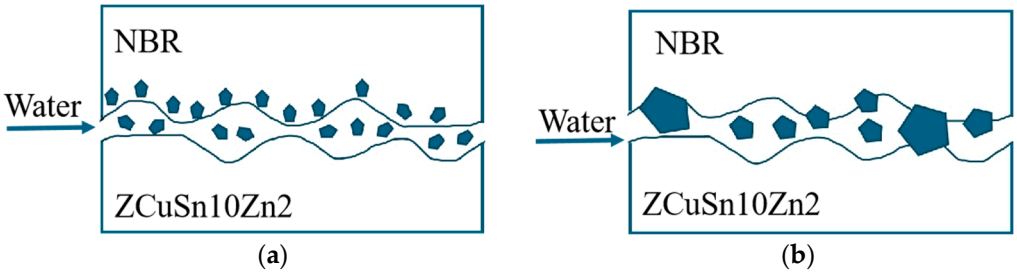


Figure 8. Wear mechanism diagram of NBR under the influence of particle size. (**a**) NBR wear mechanism diagram under the influence of small size particles, (**b**) NBR wear mechanism diagram under the influence of large size particles.

3.3. Particle Concentration Impact Analysis

3.3.1. Trend Analysis of Friction Coefficient Under the Influence of Particle Concentration

Figure 9 depicts the relationship between varying sediment particle concentrations and the coefficient of friction. In the sediment environment characterized by a particle size of 45 μm, the average friction coefficients are recorded as 0.3524 at a sediment concentration of 1.5%, 0.43426 at 6%, and 0.03133 at 9%. The data presented in Figure 9 indicate that the influence of sediment concentration on the friction coefficient does not adhere to a uniform trend. At a sediment concentration of 1.5%, the impact of sediment concentration on the friction coefficient is more pronounced than that of sediment particle size. Given that the sediment particles are significantly larger than the thickness of the lubricant film, a certain quantity of particles disrupts the integrity of the lubricating water film. Under applied loading forces, larger sediment particles fragment into smaller particles, some of which are introduced into the friction interface, increasing the friction coefficient. As the sediment concentration escalates from 3% to 4.5%, the friction coefficient initially rises before subsequently declining, achieving a peak value at a concentration of 6%. This observation indicates that the friction coefficient reaches its maximum at a sediment concentration of 6% within a 45 μm particle environment. Conversely, a notable decrease in the friction coefficient is observed at a sediment concentration of 9%, implying that the lubricating fluid becomes saturated with a high concentration of sediment particles. In this scenario, most particles remain suspended in the aqueous solution, with only a limited number entering the friction interface and contributing to the friction and wear process, substantially reducing the friction coefficient.

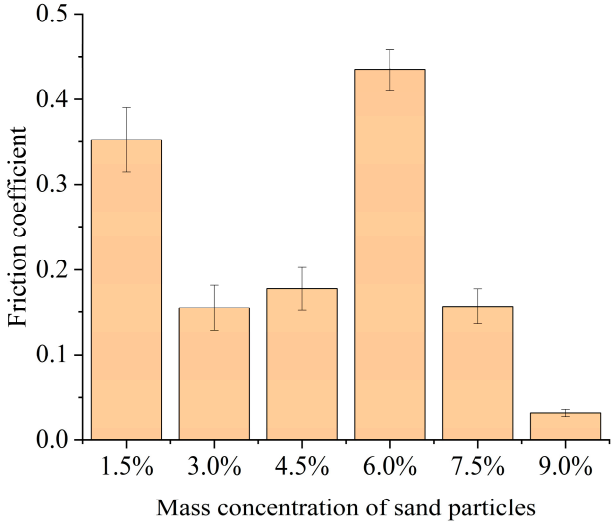


Figure 9. Results of friction coefficient under different particle concentrations.

3.3.2. Wear Volume Analysis Under the Influence of Particle Concentration

Figure 10 illustrates the influence of varying sediment particle concentrations on wear volume. The wear behavior observed at different sediment concentrations reveals distinct trends. For particles measuring 5 μm, the wear volume generally increases as the sediment concentration rises from 1.5% to higher levels; however, it peaks at a sediment concentration of 3% (refer to Figure 10a). In the case of 15 μm particles, the wear volume is susceptible to sediment concentration, with significant increases noted at concentrations of 4.5%, 7.5%, and 9% (refer to Figure 10b). This observation suggests that the NBR test blocks experience considerable wear at these concentrations, with the increase in sediment concentration exacerbating the wear phenomenon. For 25 μm particles, the wear volume exhibits minimal variation, tending to stabilize across the sediment concentration range from 1.5% to 9% (refer to Figure 10c). This indicates that the effect of sediment concentration on wear volume is negligible at this particle size, resulting in a relatively constant wear volume. When examining particles of 38 μm, the wear volume gradually increases with rising sediment concentration (refer to Figure 10d). For 45 μm particles, the wear volume is significantly higher at sediment concentrations of 1.5% and 7.5%, while it remains relatively stable and consistent at concentrations of 3%, 4.5%, 6%, and 9% (refer to Figure 10e). Lastly, 75 μm particles' wear volumes initially increase before stabilizing as the sediment concentration rises (Figure 10f).

As illustrated in Figure 10, the impact of varying solution concentrations on the wear of the NBR test block demonstrates differing sensitivities when the particle size of the sediment is held constant. For sediment particles measuring 5 μm, a saturation concentration is observed. When the sediment concentration surpasses this saturation threshold, the increase in wear becomes negligible, suggesting that at concentrations beyond this point, the majority of sediment particles remain suspended and do not significantly contribute to the wear process. In the case of 15 μm sediment particles, the thickness of the liquid film in the aqueous solution is considerably less than the particle size, resulting in the disruption of the liquid film and an imbalance between the sediment particles and the liquid film. At concentrations of 4.5%, 7.5%, and 9%, these specific sediment concentrations markedly enhance the wear of the NBR test block. For 25 μm sediment particles, although an increase in sediment concentration generally correlates with increased wear, the trend in wear volume remains relatively stable, indicating a low sensitivity of wear volume to sediment concentration at this particle size. Conversely, for 38 μm sediment particles, a linear relationship is observed between the sediment concentration and wear volume of the

NBR test block. When the particle size exceeds 38 μm, the wear volume exhibits a stable and consistent trend with increasing sediment concentration, characterized by fluctuations within a defined range.

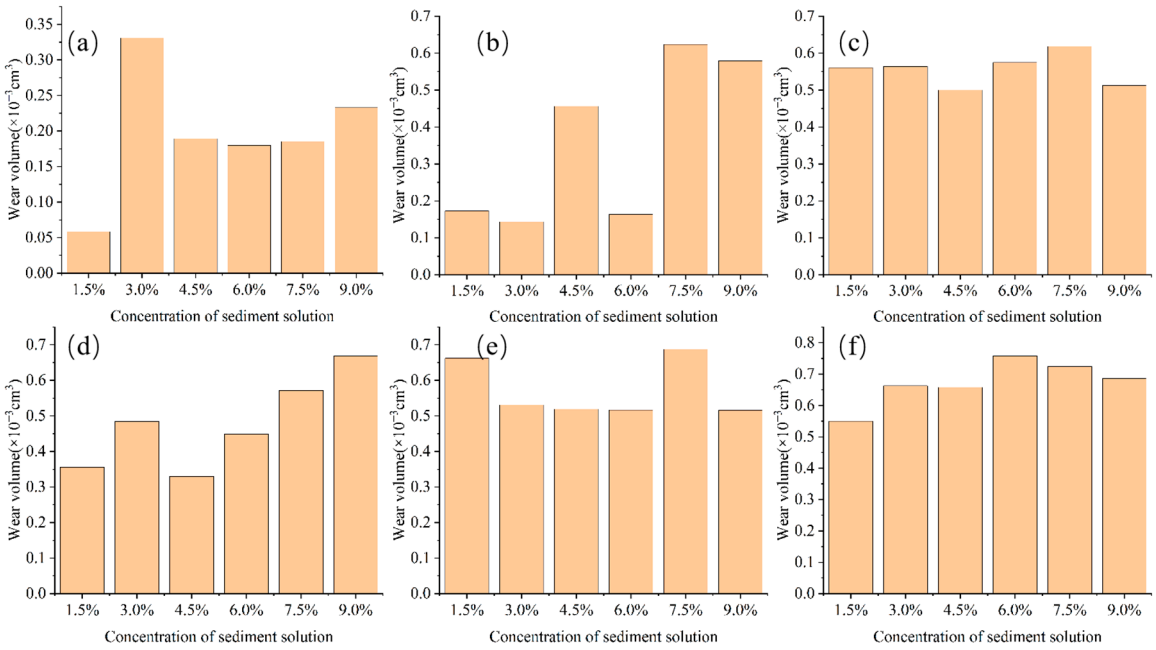


Figure 10. Wear amount under the influence of particle concentration. (**a**) At particle size 5 μm, (**b**) at particle size 15 μm, (**c**) at particle size 25 μm, (**d**) at particle size 38 μm, (**e**) at particle size 45 μm, (**f**) at particle size 75 μm.

3.3.3. Wear Surface Morphology Analysis Under the Influence of Particle Concentration

This study employed a laser confocal microscope to analyze the surface morphology of the specimens. Figure 11 illustrates the effects of varying sediment particle concentrations on the wear surface morphology under a loading force of 25 N, a linear velocity of 0.55 m/s, and a sediment particle size of 45 μm. The data in Figure 11 indicate a significant disparity in the wear outcomes of NBR specimens subjected to different sediment particle concentrations. Specifically, at a constant sediment particle size, the wear area at lower concentrations is relatively small; however, the surface exhibits a darker coloration and the presence of abrasive chips (as depicted in Figure 11a). As the concentration of sediment particles increases, the quantity of particles also rises. Nonetheless, the larger size of the sediment particles leads to some accumulation on the outer side of the friction substrate, resulting in the formation of irregular abrasion marks on both sides of the friction substrate and the development of curled abrasion chips in these regions (as shown in Figure 11b–e). Notably, when the sediment concentration reached 9%, the wear areas exhibited a lighter coloration (as illustrated in Figure 11f). This phenomenon can be attributed to the larger sizes of the sediment particles, which limited the number of particles that could penetrate the friction substrate, thereby contributing to a relatively lighter appearance of the wear surface in this context.

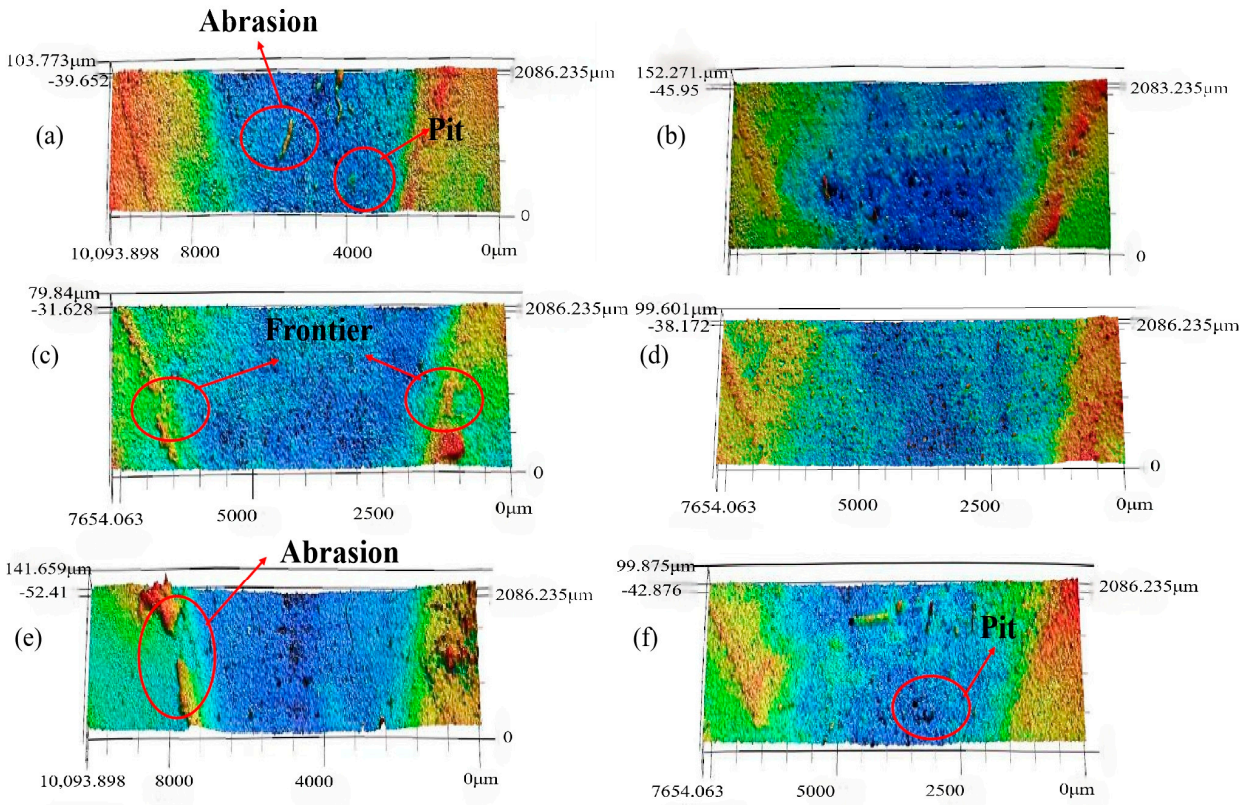


Figure 11. Wear surface morphology under the influence of particle concentration. (**a**) At 1.5% sediment concentration, (**b**) at 3% sediment concentration, (**c**) at 4.5% sediment concentration, (**d**) at 6% sediment concentration, (**e**) at 7.5% sediment concentration, (**f**) at 9% sediment concentration.

3.3.4. Wear Mechanism Analysis Under the Influence of Particle Concentration

When the particle size of the sediment is small, it approaches the thickness of the water film, resulting in the particles interacting with the friction pair primarily through a rolling motion. Some particles become embedded within the nitrile rubber's internal structure, forming smaller microscopic peaks. In contrast, others are displaced from the friction pair by the water flow movement. As the concentration of sediment particles increases, more particles accumulate between the friction pair, resulting in a significant accumulation of sediment on the surface of the friction pair. This phenomenon induces a "grinding wheel effect" between the nitrile rubber and the sediment particles, whereby the wear experienced by the nitrile rubber is considerably more pronounced than between the sediment particles and the copper ring. Figure 12 illustrates the wear mechanism of the NBR sample under conditions of low, medium, and high concentrations of slight grain-size sediment [47].

When the size of sediment particles is substantial, such that it exceeds the thickness of the water film, the presence of these particles disrupts the dynamic equilibrium between the friction surfaces. As sediment concentration increases, a portion of the particles becomes embedded in the surface of NBR due to applied loads, increasing the number of sediment particles and the formation of prominent micro-convex peaks on the NBR surface. Additionally, larger particles become embedded at the friction interface between the NBR and the copper ring, particularly at the edges of the NBR specimen. This leads to the accumulation of numerous particles, which interact with the surface of the copper ring, creating a wheel effect. The degree of abrasion experienced by the copper ring and the sediment particles is significantly greater than that between the particles and the NBR. Figure 13 illustrates the wear characteristics of the copper ring, and the interaction between particles in NBR and nitrile rubber specimens. Furthermore, Figure 13 depicts the abrasion

mechanism of NBR specimens subjected to environments with large-sized particles at low, medium, and high concentrations.

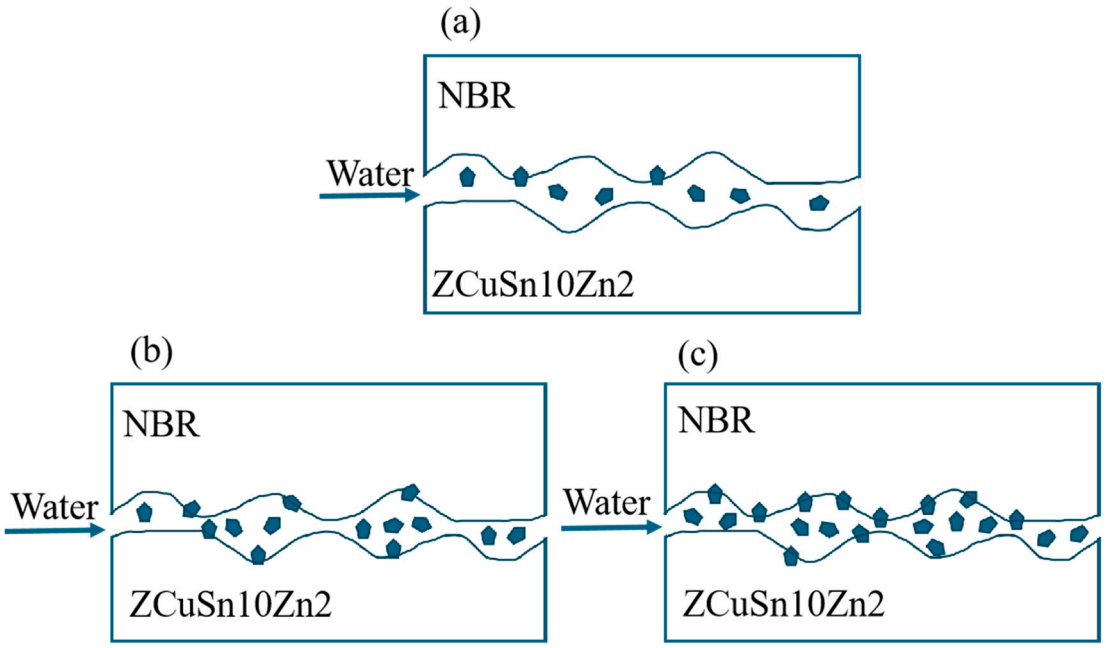


Figure 12. Wear mechanism in a small-sized particles environment with different sediment concentrations. (**a**) Low concentration. (**b**) medium concentration. (**c**) high concentration.

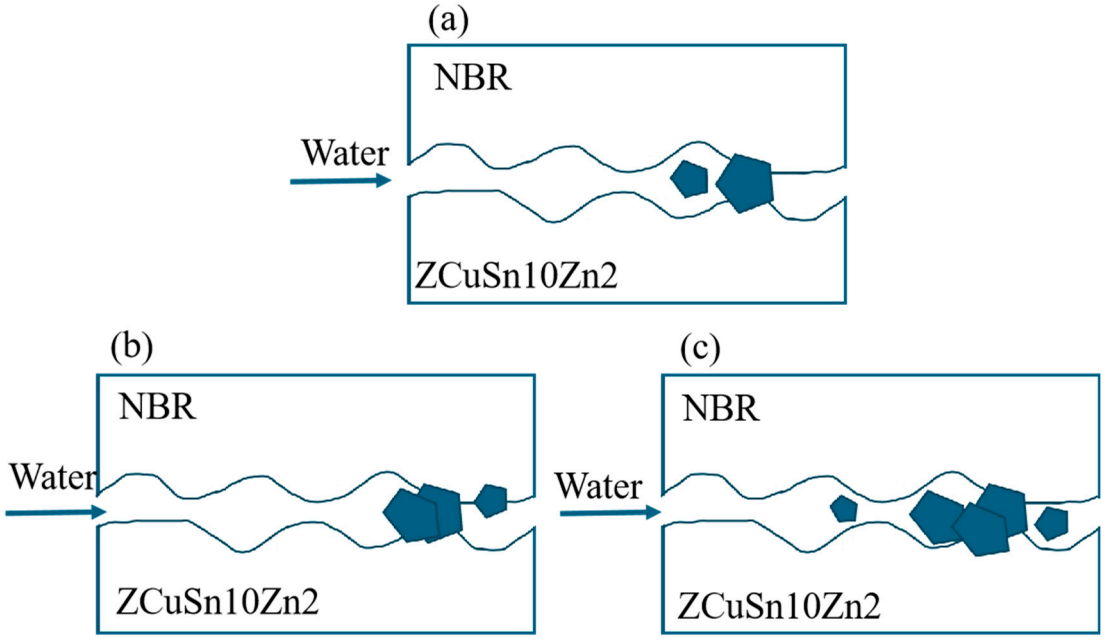


Figure 13. Wear mechanism in a large-sized particles environment with different sediment concentrations. (**a**) Low concentration. (**b**) medium concentration. (**c**) high concentration.

3.4. Synergistic Mechanism of Particle Size and Concentration on Frictional Wear Characteristics

When the sediment particles are small in size and the concentration of sediment reaches a certain threshold, the particles primarily engage in a rolling motion within the friction apparatus. As these particles traverse the NBR/copper ring friction apparatus, the degree of damage inflicted on the NBR specimen will be significantly greater than that on the copper ring. This interaction results in numerous free particles, along with a smaller proportion of sediment particles, that become embedded in the surface of the nitrile rubber,

as illustrated in Figure 14a. Conversely, when the sediment particles are more significant, the sediment concentration remains constant, and the wear mechanisms on the NBR and copper ring occur through two distinct processes—micro-cutting and rolling wear, akin to the action of a grinding wheel. In this scenario, larger sediment particles prevent some of them from entering the friction apparatus.

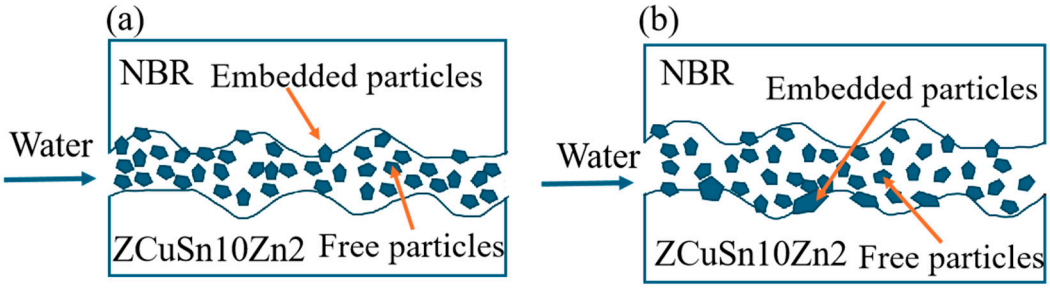


Figure 14. Schematic diagram of the synergistic mechanism. (**a**) Rolling wear model, (**b**) micro-cutting and rolling wear model.

Consequently, only a subset of the sediment particles is introduced into the friction apparatus under load. This situation alters the size effect of the particles. In an environment characterized by large particles and a high concentration, the wheel-like interaction between the particles and the copper ring is considerably more pronounced than between the particles and the nitrile rubber [48]. The corresponding micro-cutting and rolling wear model is depicted in Figure 14b.

4. Conclusions

This study investigates the synergistic effects of sediment particle size and concentration on nitrile rubber's friction and wear characteristics (NBR). Friction and wear tests of NBR in conjunction with copper rings were conducted under simulated lubrication conditions that mimic polluted water. The research comprehensively analyzes how sediment particle size and concentration influence NBR's friction and wear performance. The principal conclusions drawn from this investigation are as follows:

(1) The presence of sediment particles influences the formation of the lubricating water film, thereby impairing the friction and wear performance of the interacting surfaces;

(2) When the concentration of sediment particles is fixed, the size of the particles can either exacerbate or alleviate the wear of NBR. The particle size influences the quantity of particles that enter the friction interface. In environments characterized by small-sized particles, an increase in the concentration of sediment particles results in significantly greater wear between the NBR and the particles compared to the wear between the particles and the copper ring. Conversely, a higher sediment concentration in larger particle sizes leads to increased wear between the brass ring and the particles, surpassing the wear experienced between the particles and the NBR;

(3) The particle size alteration influences sediment particles' wear mode within a friction apparatus. In environments characterized by smaller particle sizes, sediment particles primarily engage in rolling wear, contributing to the overall wear of the friction apparatus. Conversely, in environments with larger particle sizes, sediment particles participate in wear through both micro-cutting and rolling wear mechanisms. Additionally, variations in concentration can either exacerbate or mitigate the extent of wear experienced.

Author Contributions: Conceptualization, L.W. and Q.H.; methodology, L.W. and Q.H.; software, L.W.; validation, L.W.; formal analysis, L.W.; investigation, L.W.; resources, L.W.; data curation, L.W.; writing—original draft preparation, L.W.; writing—review and editing, L.W., X.Z., Q.H., X.L., Z.Z. and S.X.; visualization, L.W.; supervision, X.Z., Q.H., X.L. and Z.Z.; project administration, X.Z., Q.H. and S.X.; funding acquisition, X.Z., Q.H. and X.L. All authors have read and agreed to the published version of the manuscript.

Funding: This study was financed by the National Natural Science Foundation of China (U2341284), the China Postdoctoral Science Foundation (GZB20240584), the Henan Province Science and Technology Research and Development Plan joint fund (242103810045), Key project research and application plan of Henan Higher Education (25A460004).

Institutional Review Board Statement: Not applicable.

Informed Consent Statement: Not applicable.

Data Availability Statement: Data are contained within the article.

Conflicts of Interest: The authors declare no conflicts of interest.

References

1. Wang, K.; Wang, J.; Huang, L.; Yuan, Y.; Wu, G.; Xing, H.; Wang, Z.; Wang, Z.; Jiang, X. A Comprehensive Review on the Prediction of Ship Energy Consumption and Pollution Gas Emissions. *Ocean Eng.* **2022**, *266*, 112826. [CrossRef]
2. Linan, D.; Du, J.; Zhang, X. The Cooperation Relationship Study on the Golden Waterway of the Yangtze River and Economic Development along the Yangtze River. *AIP Conf. Proc.* **2017**, *1890*, 040021.
3. Zhao, Y.; Zhang, Y.; Liu, X.; Wang, J. Prediction of Ground Water Environmental Impact on a Power Plant under Accident Conditions. *Environ. Earth Sci.* **2018**, *77*, 522. [CrossRef]
4. Hoang, A.T.; Pham, X.D. An Investigation of Remediation and Recovery of Oil Spill and Toxic Heavy Metal from Maritime Pollution by a New Absorbent Material. *J. Mar. Eng. Technol.* **2021**, *20*, 159–169. [CrossRef]
5. Avishai, D.; Morel, G. Experimental Investigation of Lubrication Regimes of a Water-Lubricated Bearing in the Propulsion Train of a Marine Vessel. *J. Tribol.* **2021**, *143*, 041803. [CrossRef]
6. Li, X.; Guo, Z.; Huang, Q.; Yuan, C. Insight into the Lubrication Performance of Biomimetic Porous Structure Material for Water-Lubricated Bearings. *Bionic Eng. (Eng. Ed.)* **2023**, *20*, 1905–1916. [CrossRef]
7. Zhang, Z.; Ouyang, W.; Liang, X.; Yan, X.; Yuan, C.; Zhou, X.; Guo, Z.; Dong, C.; Liu, Z.; Jin, Y.; et al. Review of the Evolution and Prevention of Friction, Wear, and Noise for Water-Lubricated Bearings Used in Ships. *Friction* **2024**, *12*, 1–38. [CrossRef]
8. Xie, Z.; Tian, Y.; Li, J.; Du, P. Lubrication Performance of a Novel Double-Film Bearing: Theory & Experiment. *Tribol. Int.* **2023**, *189*, 108958.
9. Deng, B.; Wu, H.; Yang, S.; Zhang, J. Longshore Suspended Sediment Transport and Its Implications for Submarine Erosion off the Yangtze River Estuary. *Estuar. Coast. Shelf Sci.* **2017**, *190*, 1–10. [CrossRef]
10. Zhao, Y.; Zou, X.; Liu, Q.; Wang, C.; Ge, C.; Xu, M. Clay Mineralogy Indicates the Muddy Sediment Provenance in the Estuarine-Inner Shelf of the East China Sea. *J. Asian Earth Sci.* **2018**, *152*, 69–79. [CrossRef]
11. Liu, Q.; Ouyang, W.; Li, R.; Jin, Y.; He, T. Experimental Research on Lubrication and Vibration Characteristics of Water-Lubricated Stern Bearing for Underwater Vehicles under Extreme Working Conditions. *Wear* **2023**, *523*, 204778. [CrossRef]
12. Jiang, Y.; Shi, X.; Qiu, K. A Micromechanics-Based Incremental Damage Model for Carbon Black Filled Rubbers. *Compos. Part B Eng.* **2015**, *75*, 11–16. [CrossRef]
13. Junkong, P.; Kueseng, P.; Wirasate, S.; Huynh, C.; Rattanasom, N. Cut Growth and Abrasion Behaviour, and Morphology of Natural Rubber Filled with MWCNT and MWCNT/Carbon Black. *Polym. Test.* **2015**, *41*, 172–183. [CrossRef]
14. Kueseng, P.; Sae-oui, P.; Rattanasom, N. Mechanical and Electrical Properties of Natural Rubber and Nitrile Rubber Blends Filled with Multi-Wall Carbon Nanotube: Effect of Preparation Methods. *Polym. Test.* **2013**, *32*, 731–738. [CrossRef]
15. Liu, J.; Zhang, Y.; Du, S. Effect of Friction Heat on Tribological Behaviors of Kevlar Fabric Composites Filled with Polytetrafluoroethene. *Proc. Inst. Mech. Eng. Part J J. Eng. Tribol.* **2015**, *229*, 1435–1443.
16. Lei, X.; Xiong, D.; Yang, Y.; Jin, J. Effect of Irradiation Dose on Plastic Deformation of Vacuum Hot Pressed Ultra High Molecular Weight Polyethylene. *Nucl. Instrum. Methods Phys. Res. B Beam Interact. Mater. Atoms* **2010**, *268*, 2846–2849.
17. Lin, Q.; Mao, B.; Dong, W.; Yang, F. Tribological Properties of Molybdenum Disulfide and Tungsten Disulfide Filled Modified Polytetrafluoroethylene. *Polym. Mater. Sci. Eng.* **2016**, *32*, 51–57.
18. Pei, Y.T.; Martinez-Martinez, D.; Van Der Pal, J.P.; Bui, X.L.; Zhou, X.B.; De Hosson, J.T.M. Flexible Diamond-like Carbon Films on Rubber: Friction and the Effect of Viscoelastic Deformation of Rubber Substrates. *Acta Mater.* **2012**, *60*, 7216–7225. [CrossRef]

19. Liu, J.; Liu, P.; Zhang, X.; Lu, P.; Zhang, X.; Zhang, M. Fabrication of Magnetic Rubber Composites by Recycling Waste Rubber Powders via a Microwave-Assisted in Situ Surface Modification and Semi-Devulcanization Process. *Chem. Eng. J.* **2016**, *295*, 73–79. [CrossRef]
20. Razavizadeh, M.; Jamshidi, M. Adhesion of Nitrile Rubber (NBR) to Polyethylene Terephthalate (PET) Fabric. Part 1: PET Surface Modification by Methylenediphenyl Di-Isocyanate (MDI). *Appl. Surf. Sci.* **2016**, *360*, 429–435. [CrossRef]
21. He, L.; Ma, Y.; Liu, Q.; Mu, Y. Surface Modification of Crumb Rubber and Its Influence on the Mechanical Properties of Rubber-Cement Concrete. *Constr. Build. Mater.* **2016**, *120*, 403–407. [CrossRef]
22. Shanmugharaj, A.M.; Kim, J.K.; Ryu, S.H. Modification of Rubber Surface by UV Surface Grafting. *Appl. Surf. Sci.* **2006**, *252*, 5714–5722. [CrossRef]
23. Chang, T.-L.; Yu, X.; Liang, J.F. Polydopamine-Enabled Surface Coating with Nano-Metals. *Surf. Coat. Technol.* **2018**, *337*, 389–395. [CrossRef]
24. Lu, Y.; Li, J.; Yu, H.; Wang, W.; Liu, L.; Wang, K.; Zhang, L. Plasma Induced Surface Coating on Carbon Nanotube Bundles to Fabricate Natural Rubber Nanocomposites. *Polym. Test.* **2018**, *65*, 21–28. [CrossRef]
25. Latifi, A.; Imani, M.; Khorasani, M.T.; Daliri Joupari, M. Plasma Surface Oxidation of 316L Stainless Steel for Improving Adhesion Strength of Silicone Rubber Coating to Metal Substrate. *Appl. Surf. Sci.* **2014**, *320*, 471–481. [CrossRef]
26. Karabork, F.; Akdemir, A. Friction and Wear Behavior of Styrene Butadiene Rubber-Based Composites Reinforced with Microwave-Evulcanized Ground Tire Rubber. *J. Appl. Polym. Sci.* **2015**, 132.
27. Choi, S.-S.; Kwon, H.-M.; Kim, Y.; Ko, E.; Kim, E. Determination of Bound Rubber Composition of Filled SBR/BR Blend Compounds by Analysis of the Unbound Rubber Composition and Bound Rubber Content. *Polym. Test.* **2017**, *59*, 414–422. [CrossRef]
28. Hou, C.; Gao, L.; Yu, H.; Sun, Y.; Yao, J.; Zhao, G.; Liu, Y. Preparation of Magnetic Rubber with High Mechanical Properties by Latex Compounding Method. *J. Magn. Magn. Mater.* **2016**, *407*, 252–261. [CrossRef]
29. Klein-Paste, A.; Sinha, N.K. Comparison Between Rubber–Ice and Sand–Ice Friction and the Effect of Loose Snow Contamination. *Tribol. Int.* **2010**, *43*, 1145–1150. [CrossRef]
30. Chang, Y.H.; Joo, B.S.; Lee, S.M.; Jang, H. Size Effect of Tire Rubber Particles on Tribological Properties of Brake Friction Materials. *Wear* **2018**, *394–395*, 80–86. [CrossRef]
31. Wang, Y.-Q.; Shi, X.-J.; Zhang, L.-J. Experimental and Numerical Study on Water-Lubricated Rubber Bearings. *Ind. Lubr. Tribol.* **2014**, *66*, 282–288. [CrossRef]
32. Zhimin, Y.; Xincong, Z.; Hongling, Q.; Wanying, N.; Hao, W.; Kai, L.; Yumin, T. Study on Tribological and Vibration Performance of a New UHMWPE/Graphite/NBR Water-Lubricated Bearing Material. *Wear* **2015**, *332–333*, 872–878. [CrossRef]
33. Lv, X.R.; Wang, H.M.; Wang, S.J. Effect of Swelling Nitrile Rubber in Cyclohexane on Its Ageing, Friction, and Wear Characteristics. *Wear* **2015**, *328–329*, 414–421. [CrossRef]
34. Zafar, S.; Sharma, A.K. Abrasive and Erosive Wear Behaviour of Nanometric WC–12Co Microwave Clads. *Wear* **2016**, *346–347*,29–45. [CrossRef]
35. Lee, S.H.; Yoo, S.S.; Kim, D.E.; Kang, B.S.; Kim, H.E. Accelerated Wear Test of FKM Elastomer for Life Prediction of Seals. *Polym. Test.* **2012**, *31*, 993–1000. [CrossRef]
36. Shen, M.X.; Zheng, J.P.; Meng, X.K.; Li, X.; Peng, X.D. Influence of Al_2O_3 Particles on the Friction and Wear Behaviors of Nitrile Rubber Against 316L Stainless Steel. *J. Zhejiang Univ.—Sci. A* **2015**, *16*, 151–160. [CrossRef]
37. Walker, C.I. Slurry Pump Side-Liner Wear: Comparison of Some Laboratory and Field Results. *Wear* **2001**, *250*, 81–87. [CrossRef]
38. Wang, Z.; Wang, S.; Wang, C.; Yang, F. Abrasive Erosion Wear Mechanism of Rubber in Oil Extraction Screw Pumps. *J. Shenyang Univ. Technol.* **2014**, *36*, 416–420.
39. Wang, J.; Chen, Z.; Qin, D. Study on Friction and Wear Characteristics and Mechanism of Water-Lubricated Rubber Bearings. *Lubr. Seal.* **2002**, *4*, 21–23.
40. Ren, X.; Peng, Z.; Hu, Y.; Rong, H.; Wang, C.; Fu, Z.; Qi, L.; Miao, H. Three-Body Abrasion Behavior of Ultrafine WC–Co Hardmetal RX8UF with Carborundum, Corundum, and Silica Sands in Water-Based Slurries. *Tribol. Int.* **2014**, *80*, 179–190. [CrossRef]
41. Park, S.-M.; Won, T.-Y.; Kim, G.-H.; Kim, D.-S.; Lee, Y.-Z. Effect of Dust Particle Inflow on the Wear of Rubber Seal Material in Automobile Chassis System. *Tribol. Trans.* **2010**, *54*, 87–95. [CrossRef]
42. Liang, X.; Yang, Z.; Liu, Z.; Li, J.; Yuan, Q.; Gao, H. Experimental Study on Abrasive Wear of Rubber Materials and Toughened Zirconia Ceramics Friction Pair. *Lubr. Seal.* **2003**, *39–40*, 42.
43. Liu, S.T.; Dong, C.L.; Yuan, C.Q.; Yang, Z.Y.; Wu, Y.H. Study on the effect of physical properties of three typical ship bearing composite materials on tribological behavior. *Tribol. Lett.* **2018**, *65*, 528–536.
44. Zhang, Y.; Biboulet, N.; Venner, C.H.; Lubrecht, A.A. Prediction of the Stribeck curve under full-film elastohydrodynamic lubrication. *Tribol. Int.* **2019**, *149*, 105569. [CrossRef]

45. Hu, G.; Ma, J.; Yuan, G.; Shen, K.; Wang, H. Effect of hard particles on the tribological properties of hydrogenated nitrile butadiene rubber under different lubricated conditions. *Tribol. Int.* **2022**, *169*, 107457. [CrossRef]
46. Zou, H.; Lin, B.; Ren, X.; Li, H.; Diao, Q.; Wang, Y. Particle size effects on efficiency of surface texturing in reducing friction. *Tribol. Int.* **2022**, *171*, 107518. [CrossRef]
47. Sun, W.H.; Zhou, Q.; Zhang, K.; Zhou, Z.Y.; Qin, K.; Yuan, T.X. Tribological behavior of ultra-high molecular weight polyethylene under abrasive particle environment. *Tribol. Lett.* **2024**, *72*, 925–936.
48. Hu, G.; Luo, H.H.; Wang, G.R.; Ma, J.B.; Zuo, R.D.; Gan, H. Effect of particle concentration on the frictional characteristics of the plunger seal in fracturing pumps. *Tribol. Lett.* **2023**, *72*, 1–20.

Disclaimer/Publisher's Note: The statements, opinions and data contained in all publications are solely those of the individual author(s) and contributor(s) and not of MDPI and/or the editor(s). MDPI and/or the editor(s) disclaim responsibility for any injury to people or property resulting from any ideas, methods, instructions or products referred to in the content.